MICAL-like1 mediates epidermal growth factor receptor endocytosis

Nancy Abou-Zeid[a,*], Rudy Pandjaitan[b,*], Lucie Sengmanivong[c,d], Violaine David[a], Gwenaelle Le Pavec[a], Jean Salamero[c,d], and Ahmed Zahraoui[a,b,†]

[a]Laboratory of Membrane Trafficking, DSV/iBiTec-S-URA2096 CNRS, CEA Saclay, 91191 Gif/Yvette, France; [b]Laboratory of Morphogenesis and Cell Signalling, UMR144 CNRS-Institut Curie Section de Recherche, 75005 Paris, France; [c]Nikon Imaging Centre, UMR144 CNRS-Institut Curie Section de Recherche, 75005 Paris, France; [d]Cell and Tissue Imaging Facility (IBiSA), UMR144 CNRS-Institut Curie Section de Recherche, 75005 Paris, France

ABSTRACT **Small GTPase Rabs are required for membrane protein sorting/delivery to precise membrane domains. Rab13 regulates epithelial tight junction assembly and polarized membrane transport. Here we report that Molecule Interacting with CasL (MICAL)-like1 (MICAL-L1) interacts with GTP-Rab13 and shares a similar domain organization with MICAL. MICAL-L1 has a calponin homology (CH), LIM, proline rich and coiled-coil domains. It is associated with late endosomes. Time-lapse video microscopy shows that green fluorescent protein–Rab7 and mcherry-MICAL-L1 are present within vesicles that move rapidly in the cytoplasm. Depletion of MICAL-L1 by short hairpin RNA does not alter the distribution of a late endosome/lysosome-associated protein but affects the trafficking of epidermal growth factor receptor (EGFR). Overexpression of MICAL-L1 leads to the accumulation of EGFR in the late endosomal compartment. In contrast, knocking down MICAL-L1 results in the distribution of internalized EGFR in vesicles spread throughout the cytoplasm and promotes its degradation. Our data suggest that the N-terminal CH domain associates with the C-terminal Rab13 binding domain (RBD) of MICAL-L1. The binding of Rab13 to RBD disrupts the CH/RBD interaction, and may induce a conformational change in MICAL-L1, promoting its activation. Our results provide novel insights into the MICAL-L1/Rab protein complex that can regulate EGFR trafficking at late endocytic pathways.**

Monitoring Editor
Jean E. Gruenberg
University of Geneva

Received: Jan 11, 2011
Revised: Jul 8, 2011
Accepted: Jul 18, 2011

This article was published online ahead of print in MBoC in Press (http://www.molbiolcell.org/cgi/doi/10.1091/mbc.E11-01-0030) on July 27, 2011.

The human MICAL-L1 nucleotide sequence has been deposited at the EMBL database under the accession number AJ496196.

*These authors contributed equally to this work.

†Present address: INSERM U.1016-CNRS UMR8104, Institut Cochin, F-75014 Paris, France.

Address correspondence to: A. Zahraoui (zahraoui@cea.fr).

Abbreviations used: 3D, three-dimensional; CCD, charge-coupled device; CH, calponin homology; CHX, cycloheximide; EGFR, epidermal growth factor receptor; EST, expressed sequence tag; GFP, green fluorescent protein; GST, glutathione S-transferase; ICA, intensity correlation analysis; Lat A, Latrunculin A; mAb, monoclonal antibody; MDCK, Madin–Darby canine kidney; MICAL, Molecule Interacting with CasL; MICAL-L1, MICAL-like1 ; MIP , maximum intensity projection; ORF, open reading frame; PBS, phosphate-buffered saline; PKA, protein kinase A; PRD, proline-rich domain; RBD, Rab13 binding domain; RNAi, RNA interference; shRNA, short hairpin RNA; Tf, transferrin; TfR, transferrin receptor; TGN, *trans*-Golgi network; VASP, vasodilator-stimulated phosphoprotein; WT, wild type.

INTRODUCTION

Epithelial cells exhibit distinct apical and basolateral plasma membranes separated by tight junctions that establish an apicolateral barrier to prevent intermixing of proteins and lipids between apical-lateral membranes. The maintenance of the apico-/basolateral polarity requires sorting and correct delivery of membrane proteins during exocytic and endocytic pathways. Small Rab GTPases regulate various steps of membrane trafficking. They cycle between GTP-bound active and GDP-bound inactive forms. In their active conformation, Rab proteins interact with a variety of effectors to control different cellular processes, such as vesicle sorting/targeting, vesicle movement, or kinase activities (Zahraoui *et al*., 2000; Zerial and McBride, 2001; Tisdale, 2003; Stenmark, 2009). Rab13 is closely related to Rab8, Rab10, and to the *yeast* Sec4, which is required for polarized transport in yeast (Guo *et al*., 1999). Rab8, Rab10, and Rab13 regulate surface delivery of membrane proteins to the basolateral side of epithelial cells. In addition, Rab10 regulates sorting of internalized cargos (Huber *et al*., 1993; Ang *et al*., 2003; Babbey *et al*., 2006; Schuck *et al*., 2007; Henry and Sheff, 2008; Nokes *et al*.,

2008). Rab13 is recruited to cell–cell contacts from a cytosolic pool at an early stage during the assembly of junctional complexes, suggesting a role for Rab13 in the regulation of cell–cell junctions and/or polarity in mammalian cells (Zahraoui *et al.*, 1994; Sheth *et al.*, 2000). By generating Madin–Darby canine kidney (MDCK) cell lines expressing either active (Rab13Q67L) or inactive (Rab13T22N) mutants of Rab13, we previously showed that expression of the active, but not the inactive, mutant affects the recruitment of tight junction proteins, claudin-1, occludin, and ZO-1 (Marzesco *et al.*, 2002). Moreover, we demonstrated that GTP-bound Rab13 directly binds to protein kinase A (PKA) and inhibits PKA-dependent phosphorylation of vasodilator-stimulated phosphoprotein (VASP), an actin remodeling protein. Activation of PKA blocks the inhibitory effect of Rab13 on the recruitment of VASP, ZO-1, and claudin-1 to cell–cell junctions (Kohler *et al.*, 2004). Rab13 has also been implicated in occludin recycling (Morimoto *et al.*, 2005)

To obtain further insight into the role of Rab13, we searched for Rab13 interacting proteins in a yeast two-hybrid screen. We isolated a cDNA encoding MICAL-like1, a human protein that has a domain organization similar to that of MICAL (Molecule Interacting with CasL). MICAL-like1 (MICAL-L1) interacts with Rab13 in vitro and in vivo. In epithelial MDCK cells, MICAL-L1 is localized to late endosomes and colocalizes with Rab13. Our data indicate that MICAL-L1 is a key regulator of epidermal growth factor receptor (EGFR) endocytosis in epithelial cells.

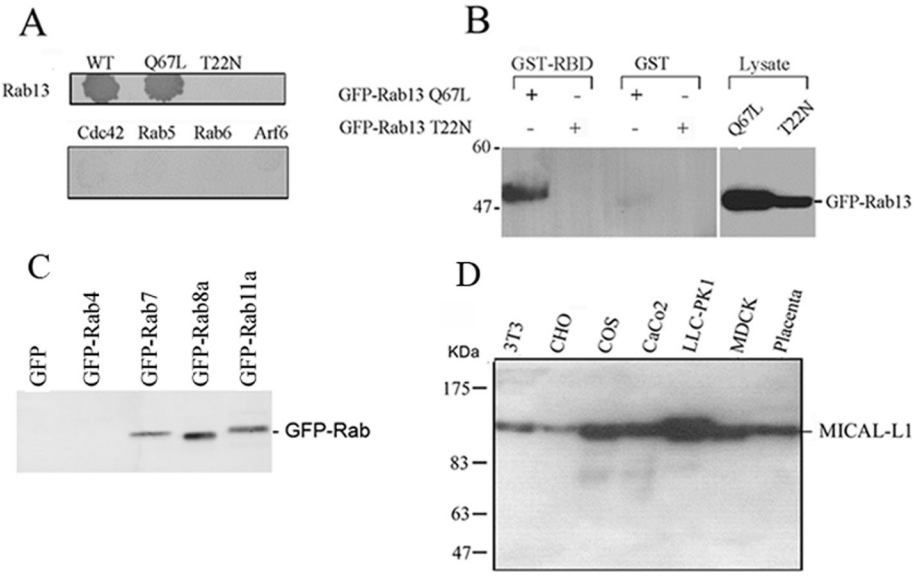

FIGURE 1: MICAL-L1 interacts with the GTP-, but not with the GDP-bound Rab13. (A) Two-hybrid interaction of RBD with Rab13. The yeast reporter strain L40 (Matα) transformed with pVJL12–RBD was conjugated by patch mating to strain Y187 (Matα) expressing cDNAs of small GTPases (indicated at top) cloned into pGAD1318. Diploid cells were plated on synthetic medium lacking leucine, tryptophan, and histidine and were grown at 30°C. Growth phenotype was determined after 48 h. RBD interacts only with the WT and the active form (Q67L) of Rab13, but not with the inactive form (T22N) of Rab13 or other small GTPases. (B) GST alone or a GST–RBD fusion protein was purified from *E. coli*, bound to glutathione beads, and incubated with cell extracts derived from MDCK cells expressing GFP–Rab13Q67L and GFP–Rab13T22N. Bound proteins were analyzed by immunoblotting with a monoclonal anti-GFP antibody. Given that GFP–Rab13Q67L was highly expressed than GFP–Rab13T22N, only 50% of GFP–Rab13Q67L lysate was incubated with GST–RBD beads. (C) GST–RBD fusion protein bound to glutathione beads and incubated with cell extracts derived from MDCK cells expressing GFP, GFP–Rab4, GFP–Rab7, GFP–Rab8, and GFP–Rab11. Bound proteins were analyzed by immunoblotting with a monoclonal anti-GFP antibody. (D) MICAL-L1 protein expression in mammalian cell lines and placenta. Total extracts (25 μg) from NIH3T3, CHO, Cos, CaCo2, LLC-PK1, and MDCK cells and placenta extract were analyzed by immunoblotting with the affinity-purified anti-RBD antibodies. MICAL-L1 was detected as a band of 116 kDa.

RESULTS

MICAL-L1 interacts with GTP-bound Rab13

To identify targets of the small GTPase Rab13, we used the active form of Rab13 (Rab13Q67L) as bait in a yeast two-hybrid screen. Eighteen clones were isolated that interacted with Rab13Q67L. Sequence analysis of these clones revealed that they were derived from the same gene and encoded a polypeptide of 300 amino acids that was named Rab13 binding domain (RBD). RBD interacted specifically with the wild type (WT) and the active form of Rab13 (Q67L), but not with the inactive mutant Rab13T22N. Furthermore, it did not bind to other small GTPases, such as Rab5, Rab6, Cdc42, and Arf6 (Figure 1, A–C). A human, full-length cDNA clone was identified that encompassed the RBD sequence and coded for a protein identical to MICAL-L1 (Supplemental Figure S1A). The interaction of MICAL-L1 and Rab13 has been reported by Yamamura *et al*. (Yamamura *et al.*, 2008). MICAL-L1 has a single calponin homology (CH) domain of 102 amino acids, a domain also found in cytoskeletal and signal transduction proteins and known to be involved in actin filament binding (Banuelos *et al.*, 1998). Adjacent to this motif, MICAL-L1 has a LIM domain, a cysteine-rich module found in numerous proteins involved in signal transduction and cytoskeletal organization (Petit *et al.*, 2003). The intermediate part of the protein is a proline-rich domain (PRD) that shares no significant similarity with MICAL or other known proteins. Finally, two putative coiled-coil structures were identified at the COOH terminus of MICAL-L1 within the RBD. In mammals, there are at least two members of the MICAL-like family, MICAL-L1 and MICAL-L2. The homology between these proteins is restricted to the CH, LIM, and C-terminal RBD domains (Supplemental Figure S1B). Glutathione *S*-transferase (GST) pull-down experiments were used to confirm the interaction obtained in the two-hybrid assay. Figure 1B shows that GST–RBD bound Rab13Q67L, but not Rab13T22N. As a control, GST alone did not interact with green fluorescent protein (GFP)–Rab13 mutants. Interestingly, GST–RBD also bound Rab7, Rab8, and Rab11, but not Rab4 or GFP (Figure 1C). Affinity-purified antibodies raised against the GST–RBD fusion protein detected a protein band of apparent relative molecular mass ~116,000 (M_r 116 kDa), slightly greater than the predicted relative molecular mass of MICAL-L1 (M_r 100 kDa). This protein band was detected in several mammalian cell lines and in placental tissue (Figure 1D). This antibody did not work in immunofluorescence experiments. We also tested available commercial antibodies and found that they recognized additional bands by immunoblots of MDCK cell extracts (unpublished data). Our results are in agreement with those of Yamamura *et al*. (Yamamura *et al.*, 2008) and suggest that MICAL-L1 interacts with GTP-bound Rab13.

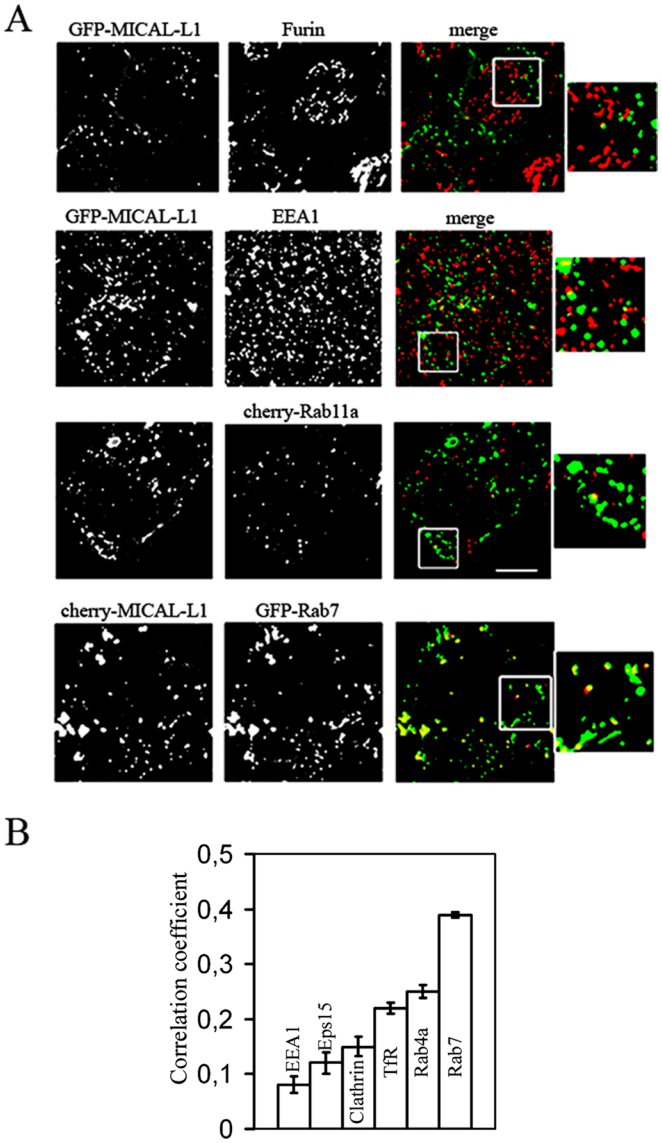

FIGURE 2: MICAL-L1 is associated with late endocytic compartments. (A) Coverslips of cells expressing GFP–MICAL-L1 or cherry-MICAL-L1 were processed for immunofluorescence using anti-furin, anti-EEA1, cherry-Rab11a, and GFP-Rab7. Three-dimensional projections of images were collected. The projections were combined into a single color image in the third column (merge). Colocalization of the two fluorophores (green and red) was revealed by the yellow color resulting from their overlapping emissions. MICAL-L1 significantly colocalizes with Rab7. The distribution of GFP–MICAL-L1 with the four endocytic markers was emphasized in the 2.0 × insets. Bar, 10 µm. (B) Intensity correlation analysis, comparing the distribution of MICAL-L1 with Rab7, Rab4a, TfR, clathrin, or Eps15 and EEA1 from 3D projection images of cells. The correlation coefficients of double labels were then calculated on deconvolved images with ICA as indicated in *Materials and Methods*. The distribution of MICAL-L1 is significantly correlated with late endocytic compartments associated with Rab7. ICA was performed on full image fields of reconstituted MIP of 3D stacks of at least 10 planes. At least five (and up to 10) double-labeled cells were analyzed in each field. Average quantification as shown in bar graphs was done on at least three different experiments.

MICAL-L1 localizes to a late endocytic compartment

The cellular distribution of GFP–MICAL-L1 was examined by immunofluorescence in epithelial MDCK cells. GFP–MICAL-L1 was detected in vesicle-like structures spread throughout the cytoplasm. A pool of MICAL-L1 was also detected at the cell periphery (Figure 2A). To compare the distribution of MICAL-L1 with well-characterized markers of intracellular trafficking, we expressed GFP–MICAL-L1 in MDCK cells. GFP–MICAL-L1 was found in vesicular compartments that did not correspond to the *trans*-Golgi network (TGN). Three-dimensional (3D) images collected of MDCK cells expressing GFP–MICAL-L1 showed that the vesicular distribution of the protein was clearly distinct from that of the furin, a marker of the TGN (Figure 2A). We then investigated whether the vesicular structures associated with GFP–MICAL-L1 were endosomes. GFP–MICAL-L1–expressing cells were costained with several markers of endocytic pathways, such as EEA1 (a marker for early endosomes), Rab7 (a late endosomal marker), and Rab11a (a recycling endosome marker). Other markers, such as transferrin receptor (TfR), clathrin, Eps15, and Rab4a, were also used (Supplemental Figure S2). MICAL-L1 localized to vesicle structures that showed significant overlap with GFP–Rab7 (Figure 2A). It showed a weak colocalization with Rab4a, Epsin15, and clathrin (Supplemental Figure S2), but was not detected in early endosomes or recycling endosomes involved in the slow recycling process as assessed by colocalization with EEA1 and Rab11a, respectively (Figure 2A and Supplemental Figure S2). These data strongly suggest that MICAL-L1 resides in late endocytic compartments. We did not succeed in assessing these features on the ultrastructural level as anti-MICAL-L1 and anti-GFP antibodies were not functional for electron microscopic analysis. To quantify the codistribution of GFP–MICAL-L1 with Rab7, Rab4a, TfR, clathrin, Eps15, and EEA1, 3D image projection cross-correlation analysis was conducted on maximum intensity projection (MIP) of 3D stacks of images as indicated in *Materials and Methods*. Consistent with our visual analysis, we found that the distribution of MICAL-L1 was significantly coincident with GFP–Rab7 and, to a lesser extent, with Rab4, clathrin, and Eps15 (a marker of coated pits). The correlation of GFP–MICAL-L1 with EEA1 was low, suggesting a weak or no association of the protein with early endosomes (Figure 2B).

MICAL-L1 protein contains a calponin (CH) domain thought to be important for interactions with actin filaments and microtubules (Suzuki *et al.*, 2002; Terman *et al.*, 2002). We examined the effect of Latrunculin A (Lat A) or nocodazole on the distribution of GFP–MICAL-L1. Lat A is a membrane-permeant actin, monomer-sequestering drug capable of depolymerizing actin filaments (Sheff *et al.*, 2002). Treatment with Lat A disrupted stress fibers and redistributed actin to scattered dots in the cytoplasm. It also induced punctate lateral actin structures. Treatment with Lat A for 30 min altered the localization of MICAL-L1, resulting in the redistribution of MICAL-L1 as cytoplasmic tubular structures. In contrast, depolymerization of microtubules with nocodazole did not affect the localization of MICAL-L1 (Figure 3A). We then tested whether MICAL-L1 tubules formed after Lat A treatment were positive for Rab proteins. MICAL-L1 was detected as membrane tubules that overlapped extensively with Rab7, Rab8, and Rab13 (Figure 3B).

MICAL-L1 regulates EGFR trafficking

To shed light on the function of MICAL-L1, we used a vector encoding short hairpin RNAs (shRNAs) to reduce MICAL-L1 expression in MDCK cells. The shRNA vector contains a GFP reporter gene that was used as a marker for transfected cells. Three different shRNAs targeting dog MICAL-L1 mRNA sequence and a control (scrambled) sequence were expressed in stably transfected MDCK cells. We selected three clones corresponding to two different shRNA sequences that showed strong depletion of MICAL-L1 protein (Figure 4A). Clone 2, MICAL-L1-shRNA (KD3) and clone 3,

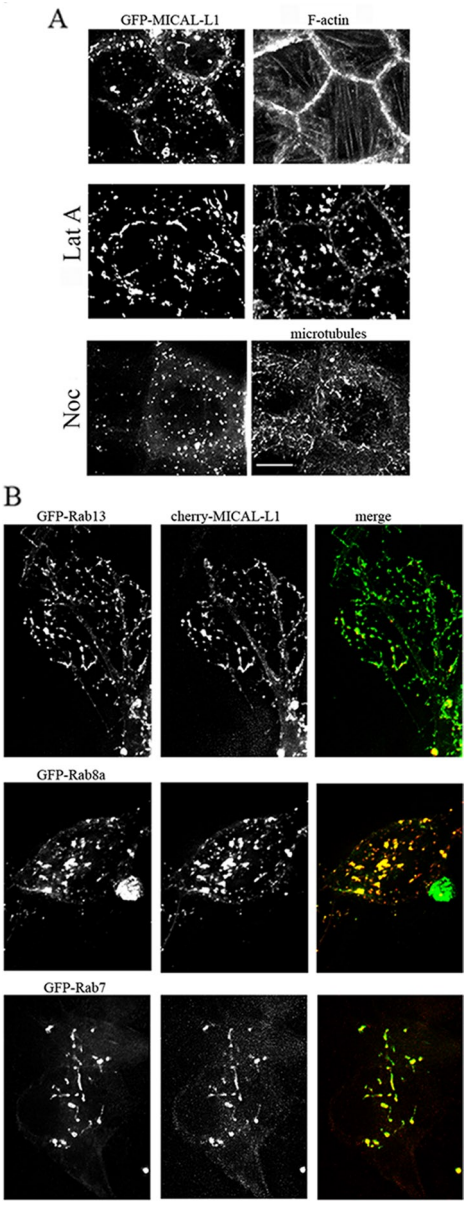

FIGURE 3: MICAL-L1 distribution depends on filamentous actin (F-actin). (A) MDCK cells expressing GFP–MICAL-L1 were treated with either Latrunculin A (Lat A) or nocodazole (Noc) and processed for immunfluorescence with phaloidin or with anti–α-tubulin. Three-dimensional stacks were acquired by 3D deconvolution microscopy. Three-dimensional projections of images are shown. (B) MDCK cells coexpressing mcherry-MICAL-L1 and either GFP–Rab7, GFP—Rab8a, or GFP–Rab13 were treated with Lat A and processed for immunofluorescence. Three-dimensional stacks were acquired by 3D deconvolution microscopy. Three-dimensional projections of images are shown. Bar, 10 μm.

scramble (Scr1 as a control) were chosen for subsequent studies. We first investigated whether MICAL-L1 silencing affected the localization of cell–cell junction proteins. Knocking down MICAL-L1 expression did not significantly affect the localization of claudin-1, occludin, ZO-1, and E-cadherin (Figure 4B). Three-dimensional images showed that, in control and KD3 cells, claudin-1 and occludin were found at the lateral plasma membrane and as a punctate staining in the cytoplasm. MICAL-L1 silencing did not alter Lamp1 (a late endosome–lysosome membrane protein) or Eps15 distribution (Figure 4B and Supplemental Figure S3).

Given the association of MICAL-L1 with late endosomes, we examined whether MICAL-L1 controls transferrin (Tf) and EGFR endocytosis. To monitor the transport of Tf, MDCK cells on coverslips expressing GFP, GFP–MICAL-L1, Scr, and MICAL-L1-shRNA were subjected to "pulse-chase" experiments with biotinylated Tf. After the pulse, all cell lines analyzed exhibited similar distribution of Tf. After 30-min chase, GFP–MICAL-L1 expression or MICAL-L1 depletion did not alter Tf distribution. A cytoplasmic accumulation of Tf was observed (Figure 5). We analyzed Tf distribution in two other independent Scr and KD clones that exhibited similar results (unpublished data). MICAL-L1 has been implicated in TfR recycling in HeLa cells. These studies were based on transfection of MICAL-L1 siRNA for 72 h in HeLa cells (Sharma *et al.*, 2009), in contrast to our studies, which were based on stable expression or depletion of MICAL-L1 in MDCK cells. It is possible that MICAL-L1 have additional functions in nonepithelial cells.

We then investigated whether MICAL-L1 affected the trafficking of EGFR. Ligand binding to EGFR at the cell surface leads to rapid internalization of EGFR complexes in early endosomes. Receptors are sorted at early endosomes, where, instead of being recycled, EGFR can be targeted to lysosomes for degradation. Receptors that are targeted to lysosomal degradation are distinguished from those destined for recycling by covalent addition of ubiquitin to the cytosolic domain of the EGFR (Sigismund *et al.*, 2005, 2008; Huang *et al.*, 2006; Roxrud *et al.*, 2008).

Because ubiquitination is required for sorting/targeting EGFR to degradation, we then tested whether MICAL-L1 affects the EGFR ubiquitination. Cells were untreated or treated with EGF for 2 min at 37°C to stimulate maximum EGFR ubiquitination. EGFRs were immunoprecipitated using a monoclonal antibody (mAb) against the extracellular domain of the receptor, separated by SDS–PAGE and immunoblotted with anti-ubiquitin antibodies. Figure 6A shows that, in all cell lines analyzed, EGFR was ubiquitinated to a similar extent, suggesting that ubiquitination of the EGFR was not affected by MICAL-L1. We also assessed the biochemical EGFR degradation in MDCK cells expressing Scr or MICAL-L1-shRNA. Indeed, cells depleted of MICAL-L1 (KD3) exhibited a substantial EGFR degradation compared with control cells (Figure 6, B and C). These results are consistent with the possibility that MICAL-L1 plays a role in EGFR trafficking at a late step in the endocytic pathway.

In addition, immunofluorescence-based pulse-chase assays with EGF were performed. After a 15-min pulse, the distribution of endogenous EGFR was not affected by expression or depletion of MICAL-L1 as compared with control cells. The receptor was clearly detected as vesicular structures at perinuclear regions (Figure 7). This perinuclear accumulation was also observed after a 1-h chase. After a 3-h chase, the EGFR was still accumulated at a perinuclear endosomal compartment in control cells as well as in cells expressing GFP–MICAL-L1. In contrast, MICAL-L1–depleted cells exhibited different EGFR distribution. EGFR vesicles were not detected at the perinuclear region but were found in vesicles spread throughout the cytoplasm (Figure 7). These results suggest that MICAL-L1 is required for EGFR trafficking at late stages of endocytosis. We also examined the influence of mock or MICAL-L1 depletion when a lower concentration of EGF was used (2 ng/ml). No significant differences between cells were observed (unpublished data).

Reintroduction of shRNA-resistant MICAL-L1 restores the perinuclear accumulation of EGFR in MICAL-L1–depleted cells

We then checked that the effect of MICAL-L1-shRNA on EGFR trafficking was specifically caused by knockdown of MICAL-L1. For this

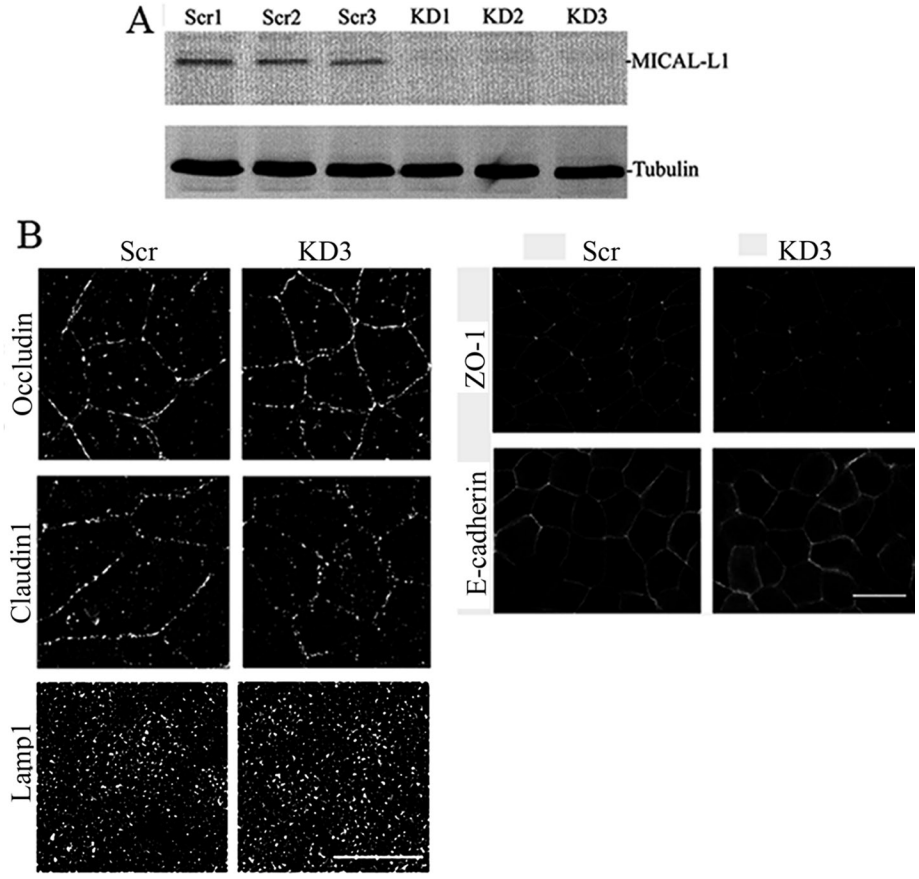

FIGURE 4: Knocking down MICAL-L1 does not affect the distribution of cell–cell junction proteins and Lamp1. Epithelial MDCK cells were stably transfected with shRNA targeted to dog MICAL-L1 mRNA sequence indicated as KD or mock-transfected indicated as scrambled (Scr). KD1 and 2 correspond to shRNA sequence 1, KD3 to shRNA sequence 2. (A) Cell lysates from the three different stable clones expressing either Scr or KD were immunoblotted with anti–MICAL-L1 antibodies. α-tubulin expression was also detected as a loading control. (B) MDCK cells expressing Scr1 or MICAL-L1 KD3 were grown on coverslips for 3 d; under these conditions, cells were not fully polarized. Cells were processed for immunofluorescence with claudin1, occludin, ZO-1, E-cadherin, and Lamp1 antibodies. Note that knocking down MICAL-L1 does not perturb the distribution of Lamp1 and cell–cell junction proteins. Three independent stable MDCK clones, KD, and three Scr clones were tested for the distribution of cell–cell junction and Lamp1 proteins. They all gave similar results. Three-dimensional projections of images are shown. Bar, 10 μm.

purpose, we transfected cells depleted of MICAL-L1 with shRNA-resistant mcherry-MICAL-L1 and performed a pulse-chase EGFR immunofluorescence experiment as indicated earlier in text. Cells were analyzed after a 3-h chase. Importantly, reexpression of mcherry-MICAL-L1 in shRNA-treated cells restored the accumulation of EGFR at the perinuclear region of cells (Figure 8A). We observed a marked accumulation of EGFR in mcherry-MICAL-L1–positive late endosomes. The overlap of EGFR with endosomes that were Rab7 positive was less important. To check that Rab7 and MICAL-L1–positive late endosomes were dynamic, we assessed their movement in living cells by using spinning confocal video fluorescence microscopy. Movement of GFP–Rab7 and mcherry-MICAL-L1 (MICAL-L1 tagged with monomeric red fluorescent protein) was observed after addition of EGF to stimulate EGFR internalization (Figure 8B and Supplementary Videos 1–3). Time-lapse video microscopy showed that GFP–Rab7 and mcherry-MICAL-L1 were present within vesicles and tubules. These vesicles exhibited linear, bidirectional, saltatory motion in the cytoplasm. In this sequence, images were collected at 500-ms intervals over a total time period of 12 min. Vesicles appeared to move rapidly in the cytoplasm with frequent pauses. They often encountered other tubulovesicular structures. GFP–Rab7 and mcherry-MICAL-L1 were thus present in a dynamic vesicular network, which corresponds to late endocytic compartments. Taken together, our data strongly suggest that at least some internalized EGFR is transported via MICAL-L1 and Rab7 endosomes. It also strengthens the notion that MICAL-L1 is required for EGFR trafficking at late endosomal compartments.

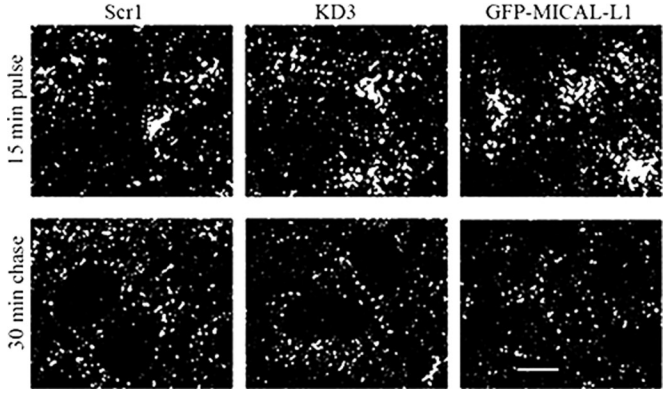

FIGURE 5: MICAL-L1 does not affect Tf distribution. Cells on coverslips were grown for 3 d, serum starved for 1 h, washed, and incubated with 25 μg/ml biotinylated holo-Tf for 30 min at 0°C. After washing, cells were pulsed for 15 min and then chased in DMEM for 30 min. Coverslips were processed for immunofluorescence. Three-dimensional stacks were acquired by 3D deconvolution microscopy. Three-dimensional projections of images are shown. Bar, 10 μm.

Rab13 colocalizes with MICAL-L1

Because MICAL-L1 interacts with the GTP-bound Rab13, we investigated whether Rab13 colocalized with MICAL-L1. Figure 9 shows that both proteins colocalized on tubulovesicular structures. Interestingly, we observed that mcherry-Rab13 exhibited a significant codistribution with GFP–Rab7 and EGFR in nonpolarized epithelial cells (Figure 9 and Supplemental Figure S4). The distribution of mcherry-MICAL-L1 was also analyzed by immunofluorescence in MDCK cells expressing GFP–Rab13Q67L, GFP–Rab13WT, or GFP–Rab13T22N (Supplemental Figure S5). In cells expressing GFP–Rab13 WT and Q67L (GTP-bound form), mcherry-MICAL-L1 decorated vesicle-like structures in the cytoplasm, and MICAL-L1 was also detected at the cell periphery. In those cells, mcherry-MICAL-L1 colocalized with GFP–Rab13 WT and Q67L. In contrast, in cells expressing the inactive mutant GFP–Rab13T22N, mcherry-MICAL-L1 was observed as tubulovesicular structures that did not colocalize with GDP–Rab13 mutant. Importantly, MICAL-L1 was not detected at the cell periphery (Supplemental Figure S5). These results are consistent with the interaction of MICAL-L1 with GTP–Rab13.

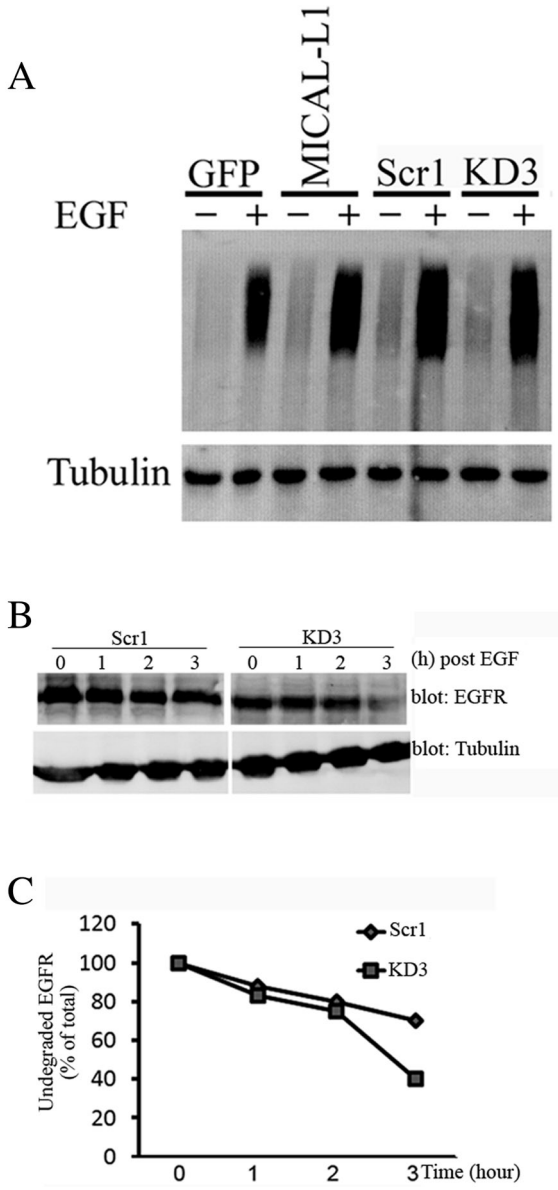

FIGURE 6: Effect of MICAL-L1 on EGFR ubiquitination and degradation. (A) Cells were untreated or treated with EGF for 2 min at 37°C. EGFR was immunoprecipitated by using an mAb against the extracellular domain of the receptor. Equal amounts of proteins were separated by SDS–PAGE and immunoblotted with anti-ubiquitin antibodies. Tubulin was detected as a loading control. (B) Cells were serum starved for 4 h in the presence of 40 μg/ml CHX, and stimulated with 100 ng/ml EGF for 15 min in the presence of CHX. They were washed and chased for the indicated time periods. They were lysed, and endogenous EGFR was analyzed by immunoblotting using polyclonal anti-EGFR antibodies. (C) Quantification of three independent experiments performed as in B. After blotting, EGFR bands were quantified using the ImageJ program and Microsoft Excel software.

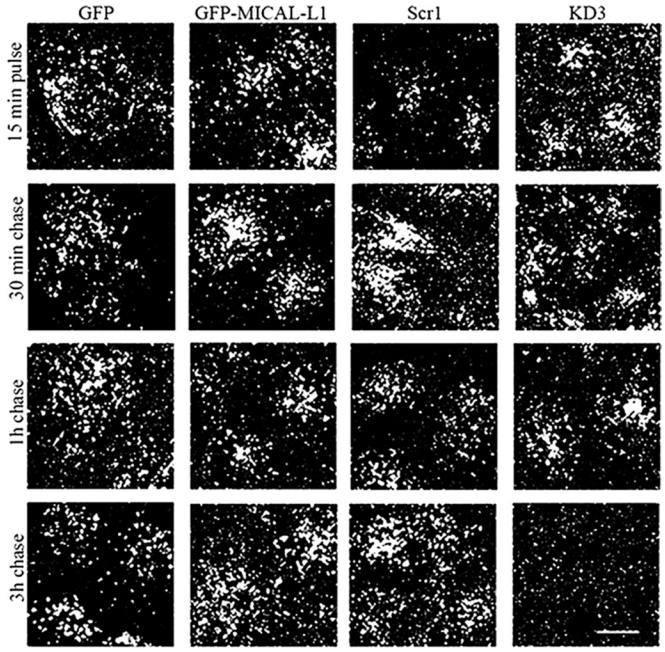

FIGURE 7: MICAL-L1 affects EGFR distribution. Stable MDCK cells expressing GFP, Scr1 (as control), MICAL-L1 shRNA (KD3), or GFP–MICAL-L1 were serum starved for 16 h, pretreated with CHX, and incubated with 100 ng/ml EGF in the presence of CHX. Cells were then pulsed for 15 min at 37°C, washed, and chased in low serum medium plus CHX for the indicated time periods. They were washed and stripped with acidic buffer to remove surface labeling. Cells were then analyzed by immunofluorescence, and 3D stacks were acquired by 3D deconvolution microscopy. Three-dimensional projections of images are shown. EGFR staining was detected mainly at a perinuclear region after a 15-min EGF pulse, or after a 1-h chase. After a 3-h chase, MICAL-L1–depleted cells exhibited a different EGFR distribution. The receptor was distributed in vesicles spread throughout the cytoplasm. Bar, 10 μm.

Interaction of the N-terminal and C-terminal regions of MICAL-L1

Given that MICAL-L1 has an inhibitory effect on EGFR trafficking, we hypothesized that MICAL-L1 exists as an inactive form due to an intramolecular interaction. First, we used the yeast two-hybrid assay to test the interaction of MICAL-L1 with a truncated version containing CHLPRD (calponin-LIM-prolin rich) domains of MICAL-L1. We did not detect any interaction between these two protein constructs (unpublished data). We then tested in vitro whether the NH2- and COOH-terminal regions of WT MICAL-L1 interacted physically. We performed a GST pull-down assay using the C-terminal RBD fused to GST. The MICAL-L1 constructs used in the interaction studies are shown in Figure 10A. GST alone or GST–RBD were immobilized on glutathione beads and incubated with MDCK cell lysate derived from cells expressing GFP, GFP–CHL (calponinLIM domains), GFP–PRD, and GFP–RBD. The proteins retained on the beads were separated on SDS–PAGE and blotted with an antibody against GFP. GST–RBD retained only the N-terminal CHL domain of all the constructs examined, whereas the GST control retained none (Figure 10B). Thus the C-terminal RBD region of MICAL-L1 binds to the N terminus. We next determined whether binding of Rab13 to the C terminus of MICAL-L1 inhibits the interaction of RBD and CH. The CH domain was expressed as a His–CH fusion protein and was incubated with GST–RBD beads. Figure 10C confirms the direct interaction of RBD and CH domains and reveals that the CH domain is sufficient for binding to the C terminus of MICAL-L1. The addition of increasing amounts of GTPγS-loaded His–Rab13 protein efficiently competed with binding of the CH to GST–RBD, thus indicating that CH/RBD interaction was controlled by GTP–Rab13. These data strengthen the idea that binding of Rab13 to MICAL-L1–RBD induces a conformational change in MICAL-L1 leading to its activation.

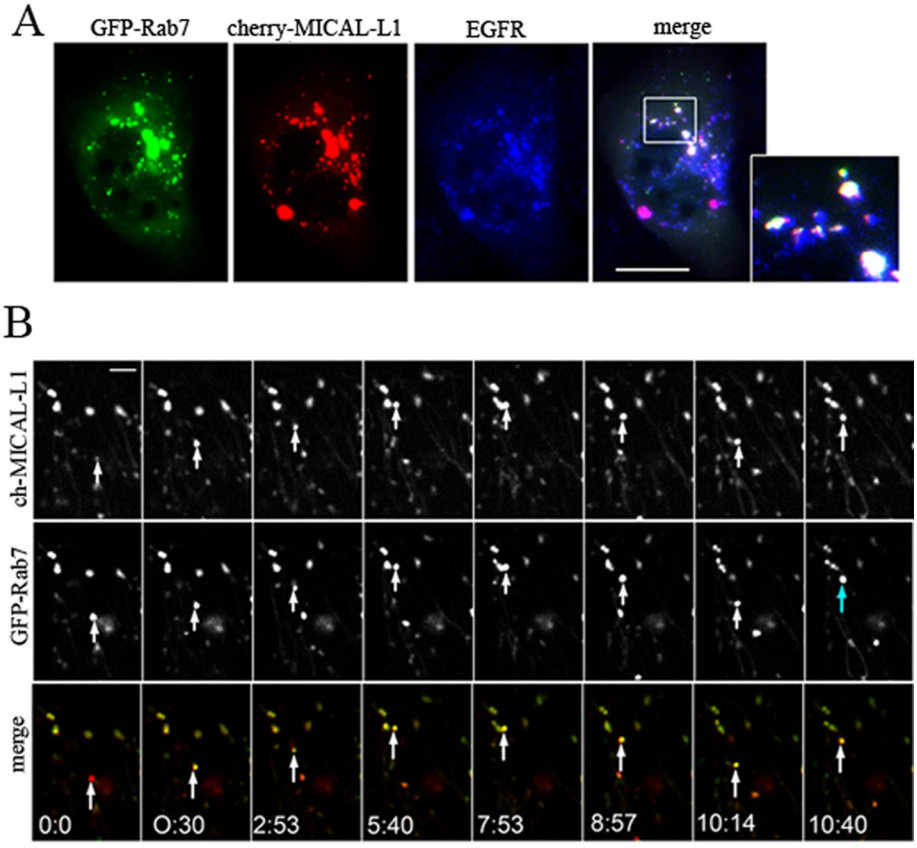

FIGURE 8: Overexpression of cherry-MICAL-L1 leads to EGFR accumulation at late endosomes. (A) MICAL-L1–depleted cells were cotransfected with shRNA-resistant cherry-MICAL-L1 and GFP–Rab7, subjected to EGF stimulation for 15 min, and chased for 3 h. Cells were fixed and stained with anti-EGFR (blue). Three-dimensional stacks were acquired by 3D microscopy, and 3D projections of images are shown. Triple colocalization is indicated in white. Inset shows magnified example of colocalization. EGFR largely accumulated in cherry-MICAL-L1–positive endosomes. A partial overlap of EGFR and GFP–Rab7–positive and cherry-MICAL-L1 late endosomes was noticed. Bar, 10 μm. (B) MDCK cells transiently cotransfected with GFP–Rab7 and mcherry-MICAL-L1 were stimulated with EGF as in A. Cells were imaged by video spinning confocal microscopy at 37°C. Images were collected at 500-ms intervals (25-ms exposure per channel). A sequence of eight images (from 0 to 10 min 40 s) indicates the movement of a GFP–Rab7 and mcherry-MICAL-L1–positive late endosome. Arrows denote GFP–Rab7 and mcherry-MICAL-L1 vesicle. Bar, 2 μm. A movie containing these images (0–40 min) highlights an example of GFP–Rab7 and mcherry-MICAL-L1–positive late endosomes behavior is shown (Supplementary Movies 1–3).

We then examined the effect of the two halves of MICAL-L1, CHLPRD (calponin-LIM-PRD) and RBD, on EGFR degradation and on Rab13 localization. The CHLPRD domain contains putative SH3 (SRC Homology Domain 3) interacting motives. The RBD domain binds Rab13, Rab7, Rab8a, and Rab11a and has a NPF (Asn-Pro-Phe amino acid motive) sequence at the N terminus that is required for interaction with EHD (Epsin15 Homology domain) proteins. Supplemental Figure S6 shows that RBD and CHLPRD exhibited a significant EGFR degradation compared with control cells. This finding suggests that both domains potentially interact with key elements involved in EGFR degradation. We found that GFP–RBD domain and mcherry-Rab13 colocalized and accumulated in the perinuclear region, whereas CHLPRD exhibited a partial colocalization with Rab13. Interestingly, CHLPRD and Rab13 were excluded from the perinuclear region and were found as punctate staining in the cytoplasm and at the cell periphery (Supplemental Figure S7). These results suggest that both domains are important for MICAL-L1 function. They are consistent with Rab13/RBD interaction.

DISCUSSION

In this study, we found that MICAL-L1 is a Rab13 interacting protein. Our data from the two-hybrid screen and the in vitro pull-down assay demonstrate that the interaction of Rab13 with MICAL-L1 is biologically relevant and GTP-nucleotide dependent. As in MICAL, MICAL-L1–RBD domain shares significant homology with other coiled-coil domains in proteins of the *Ezrin, Radixin, and Moesin* (ERM) family that link plasma membrane to actin cytoskeleton (Terman *et al.*, 2002). Moreover, MICAL-L1 contains a CH and a LIM domain. LIM domains are conserved Zn^{2+} finger motifs found in a variety of proteins exhibiting diverse biological roles. They act as modular protein-binding interfaces mediating protein–protein interactions in the cytoplasm and the nucleus (Petit *et al.*, 2003). The CH domain of MICAL-L1 is highly similar to the CH domains identified in various actin-associated proteins such as α-actinin, spectrin, Vav, and IQGAPs. CH domains exist as either tandem repeats of two CH domains or as a single CH domain. Depending on their context, they are thought to be important for interactions with actin, microtubules, and cytoskeleton-associated adaptor proteins (Gimona and Mital, 1998; Suzuki *et al.*, 2002; Terman *et al.*, 2002). The presence of a CH domain in MICAL-L1 emphasizes a potential role of MICAL-L1 in actin cytoskeleton. Interestingly, MICAL-L1 distribution is F-actin dependent. Although we do not detect any interaction in vitro between actin and MICAL-L1 (Zahraoui, unpublished data), we cannot rule out the possibility that MICAL-L1 interacts with regulatory elements of the actin cytoskeleton. F-actin depolymerization induces the membrane tubulation, and tubules are associated with MICAL-L1, Rab7, Rab8a, and Rab13. Therefore we suggest that actin remodeling is important for the regulation of membrane transport mediated by MICAL-L1 and Rab7, Rab8a, or Rab13 proteins. MICAL-L1–PRD region encompasses putative proline-rich, PxxP, sequences. It was reported that the proline-rich region of MICAL interacts with the SH3 domain of CasL, a protein required for β1 integrin-induced signal transduction and actin filament organization (Terman *et al.*, 2002). Similarly, MICAL-L1 proline-rich motives could mediate interaction with SH3 domains of signaling proteins implicated in the regulation of membrane trafficking. Further investigation of MICAL-L1–PRD will be necessary to elucidate the binding partners and the signaling pathways mediated by the PRD.

Our data show that knocking down MICAL-L1 does not affect the distribution of cell–cell junction membrane proteins, suggesting that MICAL-L1 is not involved in cell–cell junction assembly. The PRD is not conserved in MICAL-L2, a protein that has a domain organization similar to that of MICAL-L1 and interacts with Rab13 and Rab8a. Therefore, MICAL-L1 and MICAL-L2 may serve different functions due to the presence of the PRD in MICAL-L1. MICAL-L2 regulates the recycling of tight junction

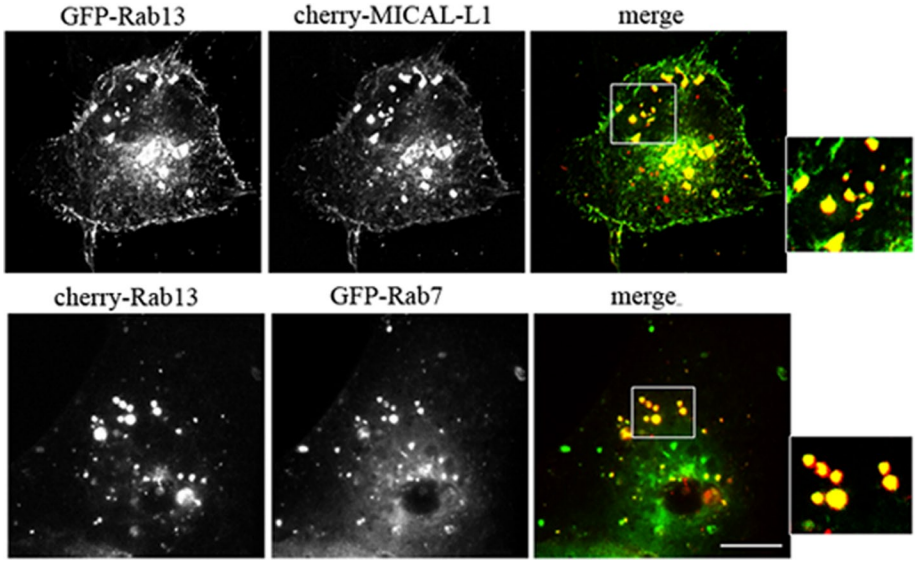

FIGURE 9: MDCK cells coexpressing GFP–Rab13/mcherry-MICAL-L1 or cherry-Rab13/GFP–Rab7 were processed for immunofluorescence. Three-dimensional stacks were acquired by 3D deconvolution microscopy. Three-dimensional projections of images are shown. Bar, 10 μm.

membrane protein, occludin (Morimoto *et al.*, 2005; Terai *et al.*, 2006; Yamamura *et al.*, 2008).

Neither silencing MICAL-L1 nor its overexpression affects EGFR ubiquitination. Importantly, silencing MICAL-L1 affects the distribution of the EGFR at a late stage of endocytosis, strengthening the notion that MICAL-L1 regulates ligand-induced receptor endocytosis. Indeed, reexpression of MICAL-L1 in MICAL-L1–depleted cells leads to the accumulation of EGFR in MICAL-L1–positive late endocytic compartments; some of these compartments also contain Rab7. Moreover, the presence of MICAL-L1 in dynamic Rab7-positive vesicles confirms that MICAL-L1 regulates trafficking of the ubiquitinated EGFR at a late step of endocytosis. It is possible that MICAL-L1 is implicated in EGFR transport between late endosomes and lysosomes because MICAL-L1 depletion stimulates EGFR degradation. It has been suggested that endosomes are organized as a mosaic of different Rab domains created through the recruitment of specific effector proteins that cooperatively act to organize membrane subdomains (Sonnichsen *et al.*, 2000; Rink *et al.*, 2005). Therefore, MICAL-L1, by binding Rab7, Rab8a, Rab11a, and Rab13, may help organize membrane domains required for cargo progression (EGFR, …) between late endocytic compartments. This hypothesis is consistent with our finding that Rab13 colocalizes with Rab7 and EGFR at least in nonpolarized cells. Further studies will be necessary to investigate the role of Rab13 in EGFR trafficking. Our results suggest that MICAL-L1 might have "open" and "closed" conformations. The two hybrid experiments (unpublished data) favors an intramolecular interaction of the N-terminal CH region with the C-terminal end (RBD domain), keeping MICAL-L1 in a closed inactive conformation. GTP–Rab13 disrupts this intramolecular interaction in a dose- dependent manner, suggesting that Rab13 binding to the RBD could induce a conformational change to convert MICAL-L1 to an open form, thereby unmasking potential sites required for the interaction of MICAL-L1 with other proteins. The interaction of MICAL-L1 with Rab13Q67L, but not Rab13T22N, and its localization as vesicles in GTP–Rab13 and as membrane tubules in GDP–Rab13 cells is in agreement with this hypothesis. This model for MICAL-L1 activation is also consistent with the fact that the RBD does not interact with MICAL-L1 protein (Zahraoui, unpublished data). A similar type of intramolecular binding, controlled by Cdc42, Rho, and Rab13, has been shown for N-WASP, mDia, and MICAL-L2 proteins, respectively (Watanabe *et al.*, 1999; Rohatgi *et al.*, 2000; Sakane *et al.*, 2010). The binding of Rab13 to MICAL-L2 promotes the recruitment of α-actinin4 to the tips of neurites. Similarly, we propose that Rab13 binding to MICAL-L1 controls MICAL-L1 intramolecular interaction to facilitate the interaction with proteins involved in the regulation of different steps of late endocytic pathways. Further investigation will be necessary to identify MICAL-L1 partners.

In conclusion, MICAL-L1, a multidomain adaptor protein, could serve as a platform for the regulation of a subset of transmembrane proteins sorting/targeting at late endocytic compartments.

MATERIALS AND METHODS

Antibodies

The purified GST–RBD protein (amino acids 690–863 of MICAL-L1) was injected into rabbits to generate polyclonal antibodies. The resulting antiserum was consecutively affinity purified on a GST column and an RBD column. mAbs against GFP were purchased from Boehringer Mannheim, (Indianapolis, IN). Anti–E-cadherin antibodies were purchased from Transduction Laboratories (San Diego, CA), anti-claudin1 and anti-TfR from Zymed Laboratories (San Francisco, CA), and rat monoclonal anti–ZO-1 antibody R40.76 was used as previously described (Anderson *et al.*, 1988). Mouse monoclonal anti-EGFR was purchased from Calbiochem (Darmstadt, Germany). Polyclonal anti-EGFR and anti-Ub were obtained from Santa Cruz Biotechnology (Santa Cruz, CA), polyclonal anti-caveolin from Transduction Laboratories (Lexington, KY), polyclonal anti-Rab13 (HPA003996) from Sigma (St. Louis, MO), and anti-Eps15 from Santa Cruz Biotechnology.

Two-hybrid screening and isolation of full-length cDNA

The yeast reporter strain L40 (Matα) was transformed with pVJL12-Rab13Q67L by electroporation. Several transformants were checked by immunoblot to determine the expression levels of the fusion protein. The clone with the highest expression level was chosen for the two-hybrid screen. A library derived from human placenta was cloned into pGAD1318 followed by transformation into the strain Y187 (Matα). Transformants (10×10^9) were conjugated to ~100×10^9 L40 cells by 8-h mass mating in liquid culture. The mating was controlled by placing aliquots under a light microscope to determine the percentage of diploids. After 8 h, the cells were plated on synthetic medium lacking leucine, tryptophan, and histidine. Finally, 35 positive clones were isolated, and inserts were sequenced, followed by comparison to the human genome. Plasmids containing sequences of interest were rescued into *Escherichia coli* HB101 cells plated on leucine-free medium. Plasmids derived from positive clones were newly transformed into Y187 cells, and another mating assay was performed. Diploids that could grow in selective medium were finally tested for β-galactosidase activity. Of the 35 positive clones, 18 contained overlapping fragments of 600 to 850 base pairs in length. The fragments were sequenced and translated in frame to the N-terminal DNA-binding domain of Lex A used for the two-hybrid screen. Thereby, a partial sequence encoding a putative open reading frame (ORF) could be detected. This sequence was named

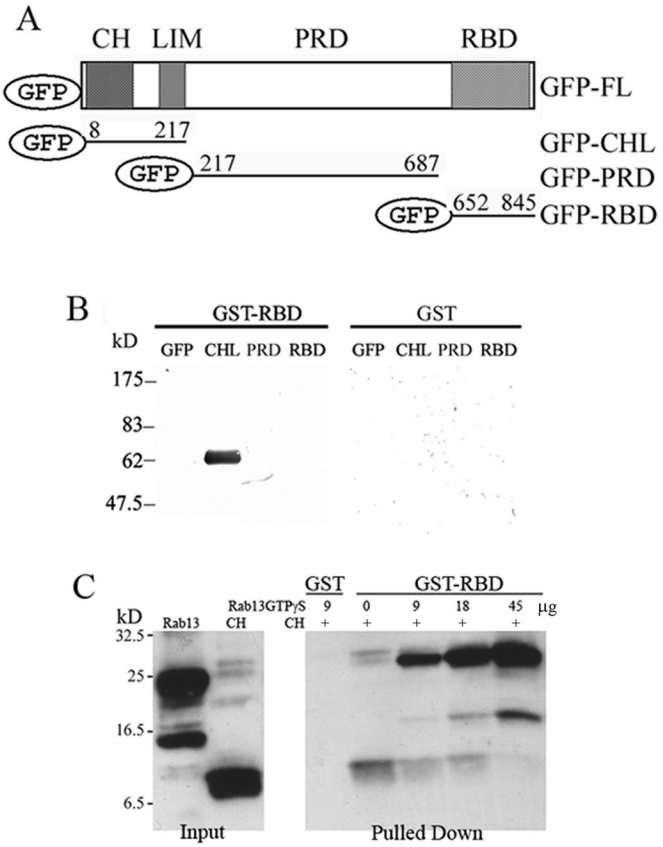

FIGURE 10: Intramolecular association of CH with RBD domain of MICAL-L1. (A) Schematic representation of GFP–MICAL-L1 constructs. Three GFP-tagged mutants, CHL (CH+LIM), PRD, and RBD and GFP-tagged WT (FL) constructs were generated. Numbers represent corresponding amino acids. (B) GST alone or GST–RBD was immobilized on glutathione beads, and incubated with lysates of MDCK expressing various GFP-tagged fragments of MICAL-L1. The proteins retained on the beads were separated on SDS–PAGE and blotted with an antibody against GFP-tag. (C) Recombinant His-Rab13 preloaded with GTPγS was mixed at various concentrations with GST–RBD beads and His-CH. Proteins bound to the beads were separated by SDS–PAGE and blotted with the anti-His antibodies. Addition of increasing amounts of GTPγS-loaded His-Rab13 protein efficiently competes with binding of the CH to GST–RBD. Left, purified His-Rab13 and His-CH proteins. The Rab13 lower band (15k) recognized by anti-His antibodies results from degradation of His-Rab13.

RBD. By sequence comparison, several EST (expressed sequence tag) cDNAs could be identified that contained the RBD sequence. The longest EST containing an insert of ~5800 base pairs was purchased from the IMAGE consortium (IMAGE clone 2262785; RZPD, Berlin, Germany) and sequenced. Sequence analysis revealed an ORF of 2586 base pairs encoding a protein of 863 amino acids.

Constructs

GFP–Rab7 was obtained from M. Arpin, mcherry-Rab11a from B. Goud, and GFP–Rab4a from P. Chavrier (Curie Institute, Paris, France). GFP–Rab8a was generated (Marzesco *et al.*, 2002). For overexpression experiments, a 3000–base pair fragment encoding the full-length MICAL-L1 was cut out of IMAGE clone 2262785 by a *Xho*I–*Xba*I digest and ligated into the corresponding sites of a pEGFP-N2 vector (Clontech, Palo Alto, CA), thereby replacing the cut-out GFP. This plasmid now contained the MICAL-L1 ORF, 68 base pairs of the 5′-untranslated region as well as 200 base pairs of the 3′-untranslated region. MICAL-L1 WT was fused to the C terminus of the enhanced GFP and cloned into the pGFP-C3 vector (Clontech). Cherry-MICAL-L1 was also generated. All constructions were verified by sequencing.

For RNA interference (RNAi), the canine MICAL-L1 cDNA sequence (XM_538381) was used to design three pairs of primers targeting different regions of canine MICAL-L1 ORF according to the manufacturer's instructions (InvivoGen, San Diego, CA). The shRNA sequences that efficiently inhibited MICAL-L1 expression were as follows: shRNA oligo sens1, 5′-ACCTCGTCG CAGTATTACAACCACTT*TCAAGAG*AAGTGGTTGTAATACT-GCGACTT-3′; shRNA oligo-antisens1, 5′ -CAAAAAGTCGCAGTATTACAACCACTT*CTCTTG*AAAGTGGTTGTAATACTGCGACG-3′; shRNA oligo sens2: 5′ ACCTCGACCTACGTGTCGCAGTATTA*TCAAGAG*TAATACTGCGACACGTAGGTCTT-3′. shRNA oligo-antisens2, 5′-CAAAAAGACCTACGTGTCGCAGTATTA*CTCTTG*ATAATACTGCGACACGTAGGTCG-3′.

Scrambled oligos sens and antisens were as follows: 5′-ACCTCGCTGTTCC TACTCGCAAATAA*TCAAGAG*TTATTTGCGAGTAGGAACAGCTT-3′, and 5′-CAAA AAGCTGTTCCTACTCGCAAATAA*CTCTTG*ATTATTTGCGAGTAGGAACAGCG-3′, respectively. Italics indicate the 7-base-pairs hairpin loop. Underlined nucleotides correspond to Bbs1 cloning sites.

Cell culture and transfection

MDCK cells (clone II) were cultured in DMEM supplemented with 10% fetal calf serum, 2 mM glutamine, 100 U/ml penicillin, and 10 mg/ml streptomycin. The cells were incubated at 37°C under a 10% CO_2 atmosphere. Cells were grown for 3 d; under these conditions, cells were subconfluent and not fully polarized. MDCK cells stably expressing GFP, GFP–Rab13T22N, or GFP–Rab13Q67L were previously described (Marzesco *et al.*, 2002). Stable MDCK cell lines expressing MICAL-L1 WT (FL) were generated by transfection using Lipofectamine 2000 Transfection Reagent according to the manufacturer's instructions (InvivoGen). Positive clones were selected and cloned in the same medium supplemented with 1 mg/ml of G418 (Life Technologies, Carlsbad, CA). Stably transfected clones were maintained under selection in 500 μg/ml of G418.

For RNAi transfection, the sense and antisense oligonucleotides were annealed and cloned into Bbs1 sites of the psiRNA-h7SK vector (InvivoGen). This vector contains zeocin resistance and encodes the GFP reporter gene used as a marker for transfected cells. The psiRNA-h7SK-scramble vector was used as a negative control. The shRNA constructs were transfected into MDCK II cells using Lipofectamine 2000 Transfection Reagent. Stable MDCK cells expressing shRNA of MICAL-L1 and scramble (control) were selected and cloned in the same medium supplemented with 0.3 mg/ml zeocin. Stably transfected clones were maintained under selection in 0.1 mg/ml zeocin.

GST pull-down assay

The GST fusion protein was constructed by inserting a *Bam*HI–*Xho*I fragment containing RBD into the corresponding sites of pGEX-4T expression vector. GST-fusion proteins were expressed in *E. coli* and purified according to the manufacturer's protocol (Amersham Pharmacia, Uppsala, Sweden). Purified GST-RBD or GST alone was bound to glutathione beads (Amersham Pharmacia) and incubated with cell extracts derived from MDCK cells expressing GFP–Rab13Q67L and GFP–Rab13T22N or GFP and GFP–MICAL-L1. The beads were washed three times with phosphate-buffered saline (PBS), and bound material was analyzed

on SDS–PAGE and immunoblotted using monoclonal anti-GFP or anti-Rab13 antibodies.

The cDNAs encoding Rab13 and CH domain (amino acids 1–102) were inserted into *E. coli* pET-15b expression vector, produced as histidine fusion proteins (His-Rab13 and His-CH), and purified on Ni^{2+}-agarose beads by classical methods.

Immunoblot and coimmunoprecipitation

Protein amounts were determined using the Bradford protocol (Bio-Rad, Munich, Germany), and protein separation in SDS–PAGE and immunoblotting were performed as described (Kohler *et al.*, 2004). Immunoblot detection was done by enhanced chemiluminescence according to manufacturer protocols (GE Healthcare Europe GmbH).

For immunoprecipitation experiments, MDCK cell lines expressing GFP–MICAL-L1 or MICAL-L1 KD were solubilized in IP buffer (50 mM Tris-HCl pH 7.6, 120 mM NaCl, 1.8 mM $CaCl_2$, 0.5% Triton X-100, protease inhibitor mix). Cell extracts were centrifuged at 15,000 × *g*, and the supernatant was incubated for 4 h at 4°C with anti-MICAL-L1 or anti-EGFR antibodies followed by the addition of protein A-sepharose. After a 2-h incubation, the beads were washed five times with IP buffer. Bound material was solubilized with SDS–PAGE sample buffer and analyzed by immunoblotting with anti-MICAL-L1, anti-GFP, or anti-ubiquitin antibodies.

Immunofluorescence microscopy

Cells grown on glass coverslips for 3 d were washed with PBS containing 1 mM calcium and 0.5 mM magnesium and fixed with 3% paraformaldehyde for 15 min. Immunofluorescence was performed essentially as described (Marzesco *et al.*, 2002). For permeabilization, cells were incubated in blocking buffer (PBS + 0.2% bovine serum albumin containing 0.1% Triton X-100). Permeabilized cells were incubated for 1 h with the primary antibodies, rinsed three times for 10 min with the blocking buffer, and then incubated with goat-affinity purified antibodies conjugated to Cy2 or Cy3 (Jackson ImmunoResearch Laboratories, West Grove, PA). After washing, samples were analyzed with a 3D microscope (see next section) and further processed with Adobe Photoshop software (Adobe Systems, Mountain View, CA).

Image acquisition, processing, and fluorescence quantification

Three-dimensional stacks with a 0.3-μm step were acquired by 3D deconvolution microscopy (Angenieux *et al.*, 2005), adapted on an Eclipse 90i upright microscope (Nikon, Paris, France) equipped with a cool SNAP HQ2 charge-coupled device (CCD) camera (Photometrics, Tucson, AZ) and using a 100X CFI Plan Apo VC objective (NA 1.4; Nikon) controlled in the *z* axis by a Piezo Objective (PI, S.A.S, Montrouge, France). All deconvolution processes were performed automatically using an iterative and measured point spread function (PSF)-based algorithm method (Gold-Meinel) on batches of image stacks, as a service proposed by the BioImaging Cell and Tissue Core Facility of the Institut Curie (PICT-IBiSA). The levels of colocalization were estimated on deconvolved images by intensity correlation analysis (ICA), basically as previously described (Li *et al.*, 2004) and by using the dedicated ImageJ plugin (Correlation Analysis Sasha), except that we did not select a particular area of the images through image segmentation in this case. Quantitative analyses of coincident structures and ICA based on their relative intensities in the different channels were performed by MIP of the multi-labeled stacks constituted of an average of eight to 15 planes each.

Video microscopy

Images were acquired on a fast scanning confocal system (with a CSU22 Yokogawa spinning-disk head) mounted on an inverted microscope (Nikon TE2000) equipped for live cell imaging (the Box: Life Imaging Service, Basel, Switzerland). Image acquisitions were performed using a 100 × Plan Apo VC 1.4 oil objective and a highly sensitive cooled interline CCD camera (CoolSnap HQ2; Roper Scientific, Paris, France). Z-dimension positioning was accomplished by a Piezo motorized stage (NanoScanZ–Piezo focusing stage; Marzhauser). Both 491- and 561-nm laser diodes (Cobolt AB, Stockholm, Sweden) interfaced with an AOTF (Accousto Optic Tunable Filter) were used for sample illumination.

Tf uptake

Cells were grown on coverslips and serum starved for 1 h. They were incubated with 25 μg/ml biotinylated holo-Tf (Sigma T-3915) for 30 min at 0°C. After washing, cells were incubated for 15 min at 37°C and chased in normal DMEM for 30 min at 37°C. Cells were processed for immunofluorescence, and biotinylated Tf was revealed by streptavidin–Texas Red.

EGFR endocytosis

Cells expressing the indicated plasmids or transfected with shRNA of MICAL-L1 were serum starved for 16 h, pretreated with cycloheximide (CHX, 40 μg/ml) at 37°C for 60 min, and then cooled to 4°C. Subsequently, 100 ng/ml EGF was applied at 4°C in the presence of CHX to allow ligand binding to the receptor. Cells were then pulsed for 15 min at 37°C, washed, and chased in low serum medium plus CHX for the indicated time. To answer visualization of internalized EGFR, coverslips were washed and stripped for 3 min at 4°C in 50 mM glycine, 100 mM NaCl, pH 3.0, to remove surface labeling and then subjected to immunofluorescence analysis.

EGFR ubiquitination

For ubiquitination, cells were serum starved for 4 h and untreated or treated with EGF (100 ng/ml) at 37°C for 2 min. Cells were washed with PBS and solubilized at 4°C in 150 mM KCl, 2 mM $MgCl_2$, 20 mM HEPES, 10% glycerol, pH 7.2, 1 mM dithiothreitol, 1 mM EGTA, 1 mM EDTA, 1 mM sodium orthovanadate, 10 mM sodium fluoride, 1 mM phenylmethylsulfonyl fluoride, 10 μg/ml leupeptin, 544 μM iodoacetamide, 10 μg/ml aprotinin containing 1% Triton X-100, and 10 mM *N*-ethylmaleimide (Huang *et al.*, 2006). Lysates were cleared by centrifugation at 14,000 × *g* for 15 min. EGFR was immunoprecipitated with mAb, separated by SDS–PAGE, and immunoblotted with anti-ubiquitin antibodies.

EGFR degradation assay

Cells were serum starved for 4 h in the presence of 40 μg/ml CHX and then stimulated with 100 ng/ml EGF in the presence of CHX for 15 min at 37°C. Cells were washed and chased in low serum medium plus CHX for the indicated time. They were lysed in 10 mM Tris-HCl, pH 7.6, 150 mM NaCl, 25 mM KCl, 1.8 mM $CaCl_2$, 1% Triton X-100, and a mixture of protease inhibitors. Cell extracts were then cleared by centrifugation, separated by SDS–PAGE, and immunoblotted with polyclonal anti-EGFR antibodies. Protein bands were quantified using ImageJ software (National Institutes of Health, Bethesda, MD)

ACKNOWLEDGMENTS

We are grateful to C. Jackson (Institut J. Monod, Paris) for critical reading of the manuscript, B. Goud (Institut Curie, Paris) for

mcherry-Rab11a, P. Chavrier (Institut Curie, Paris) for GFP-Rab4a, M. Arpin (Institut Curie, Paris) for GFP-Rab7, and A. Benmerah (Institut Cochin, Paris) for anti-Eps15. This work was supported by grants from the French National Center for Scientific Research (CNRS; AC DRAB04/140); the Commissariat à l'Energie Atomique (CEA); the Agence National de la Recherche (ANR-MICAD; NANR-08-Biot-015-01); the Institut Curie; the Association pour la Recherche sur le Cancer (ARC 5789); and the Fondation pour la Recherche Médicale (FRM). N.A.Z. and R.P. are recipients of fellowships from the CEA and FRM, respectively.

REFERENCES

Anderson JM, Stevenson BR, Jesaitis LA, Goodenough DA, Mooseker MS (1988). Characterization of ZO-1, a protein component of the tight junction from mouse liver and Madin-Darby canine kidney cells. J Cell Biol 106, 1141–1149.

Ang AL, Folsch H, Koivisto UM, Pypaert M, Mellman I (2003). The Rab8 GTPase selectively regulates AP-1B-dependent basolateral transport in polarized Madin-Darby canine kidney cells. J Cell Biol 163, 339–350.

Angenieux C *et al.* (2005). The cellular pathway of CD1e in immature and maturing dendritic cells. Traffic 6, 286–302.

Babbey CM, Ahktar N, Wang E, Chen CC, Grant BD, Dunn KW (2006). Rab10 regulates membrane transport through early endosomes of polarized Madin-Darby canine kidney cells. Mol Biol Cell 17, 3156–3175.

Banuelos S, Saraste M, Carugo KD (1998). Structural comparisons of calponin homology domains: implications for actin binding. Structure 6, 1419–1431.

Gimona M, Mital R (1998). The single CH domain of calponin is neither sufficient nor necessary for F-actin binding. J Cell Sci 111 (Pt 13) 1813–1821.

Guo W, Roth D, Walch-Solimena C, Novick P (1999). The exocyst is an effector for Sec4p, targeting secretory vesicles to sites of exocytosis. EMBO J 18, 1071–1080.

Henry L, Sheff DR (2008). Rab8 regulates basolateral secretory, but not recycling, traffic at the recycling endosome. Mol Biol Cell 19, 2059–2068.

Huang F, Kirkpatrick D, Jiang X, Gygi S, Sorkin A (2006). Differential regulation of EGF receptor internalization and degradation by multiubiquitination within the kinase domain. Mol Cell 21, 737–748.

Huber LA, Pimplikar S, Parton RG, Virta H, Zerial M, Simons K (1993). Rab8, a small GTPase involved in vesicular traffic between the TGN and the basolateral plasma membrane. J Cell Biol 123, 35–45.

Kohler K, Louvard D, Zahraoui A (2004). Rab13 regulates PKA signaling during tight junction assembly. J Cell Biol 165, 175–180.

Li Q, Lau A, Morris TJ, Guo L, Fordyce CB, Stanley EF (2004). A syntaxin 1, Galpha(o), and N-type calcium channel complex at a presynaptic nerve terminal: analysis by quantitative immunocolocalization. J Neurosci 24, 4070–4081.

Marzesco AM, Dunia I, Pandjaitan R, Recouvreur M, Dauzonne D, Benedetti EL, Louvard D, Zahraoui A (2002). The small GTPase Rab13 regulates assembly of functional tight junctions in epithelial cells. Mol Biol Cell 13, 1819–1831.

Morimoto S, Nishimura N, Terai T, Manabe S, Yamamoto Y, Shinahara W, Miyake H, Tashiro S, Shimada M, Sasaki T (2005). Rab13 mediates the continuous endocytic recycling of occludin to the cell surface. J Biol Chem 280, 2220–2228.

Nokes RL, Fields IC, Collins RN, Folsch H (2008). Rab13 regulates membrane trafficking between TGN and recycling endosomes in polarized epithelial cells. J Cell Biol 182, 845–853.

Petit MM, Meulemans SM, Van de Ven WJ, Fradelizi J, Golsteyn RM, Ayoubi TA, Menichi B, Louvard D, Friederich E (2003). The focal adhesion and nuclear targeting capacity of the LIM-containing lipoma-preferred partner (LPP) protein LPP, an actin cytoskeleton protein related to zyxin, harbors a nuclear export signal and transcriptional activation capacity. J Biol Chem 278, 2157–2168.

Rink J, Ghigo E, Kalaidzidis Y, Zerial M (2005). Rab conversion as a mechanism of progression from early to late endosomes. Cell 122, 735–749.

Rohatgi R, Ho HY, Kirschner MW (2000). Mechanism of N-WASP activation by CDC42 and phosphatidylinositol 4,5-bisphosphate. J Cell Biol 150, 1299–1310.

Roxrud I, Raiborg C, Pedersen NM, Stang E, Stenmark H (2008). An endosomally localized isoform of Eps15 interacts with Hrs to mediate degradation of epidermal growth factor receptor. J Cell Biol 180, 1205–1218.

Sakane A, Honda K, Sasaki T (2010). Rab13 regulates neurite outgrowth in PC12 cells through its effector protein, JRAB/MICAL-L2. Mol Cell Biol 30, 1077–1087.

Schuck S, Gerl MJ, Ang A, Manninen A, Keller P, Mellman I, Simons K (2007). Rab10 is involved in basolateral transport in polarized Madin-Darby canine kidney cells. Traffic 8, 47–60.

Sharma M, Panapakkam Giridharan SS, Rahajeng J, Naslavsky N, Caplan S (2009). MICAL-L1 links EHD1 to tubular recycling endosomes and regulates receptor recycling. Mol Biol Cell 20, 5181–5194.

Sheff DR, Kroschewski R, Mellman I (2002). Actin dependence of polarized receptor recycling in Madin-Darby canine kidney cell endosomes. Mol Biol Cell 13, 262–275.

Sheth B, Fontaine J, Ponza E, McCallum A, Page A, Citi S, Louvard D, Zahraoui A, Fleming TP (2000). Differentiation of the epithelial apical junctional complex during mouse preimplantation development: a role for rab13 in the early maturation of the tight junction. Mech Dev 97, 93–104.

Sigismund S, Argenzio E, Tosoni D, Cavallaro E, Polo S, Di Fiore PP (2008). Clathrin-mediated internalization is essential for sustained EGFR signaling but dispensable for degradation. Dev Cell 15, 209–219.

Sigismund S, Woelk T, Puri C, Maspero E, Tacchetti C, Transidico P, Di Fiore PP, Polo S (2005). Clathrin-independent endocytosis of ubiquitinated cargos. Proc Natl Acad Sci USA 102, 2760–2765.

Sonnichsen B, De Renzis S, Nielsen E, Rietdorf J, Zerial M (2000). Distinct membrane domains on endosomes in the recycling pathway visualized by multicolor imaging of Rab4, Rab5, and Rab11. J Cell Biol 149, 901–914.

Stenmark H (2009). Rab GTPases as coordinators of vesicle traffic. Nat Rev Mol Cell Biol 10, 513–525.

Suzuki T, Nakamoto T, Ogawa S, Seo S, Matsumura T, Tachibana K, Morimoto C, Hirai H (2002). MICAL, a novel CasL interacting molecule, associates with vimentin. J Biol Chem 277, 14933–14941.

Terai T, Nishimura N, Kanda I, Yasui N, Sasaki T (2006). JRAB/MICAL-L2 is a junctional Rab13-binding protein mediating the endocytic recycling of occludin. Mol Biol Cell 17, 2465–2475.

Terman JR, Mao T, Pasterkamp RJ, Yu HH, Kolodkin AL (2002). MICALs, a family of conserved flavoprotein oxidoreductases, function in plexin-mediated axonal repulsion. Cell 109, 887–900.

Tisdale EJ (2003). Rab2 interacts directly with atypical protein kinase C (aPKC) iota/lambda and inhibits aPKCiota/lambda-dependent glyceraldehyde-3-phosphate dehydrogenase phosphorylation. J Biol Chem 278, 52524–52530.

Watanabe N, Kato T, Fujita A, Ishizaki T, Narumiya S (1999). Cooperation between mDia1 and ROCK in Rho-induced actin reorganization. Nat Cell Biol 1, 136–143.

Yamamura R, Nishimura N, Nakatsuji H, Arase S, Sasaki T (2008). The interaction of JRAB/MICAL-L2 with Rab8 and Rab13 coordinates the assembly of tight junctions and adherens junctions. Mol Biol Cell 19, 971–983.

Zahraoui A, Joberty G, Arpin M, Fontaine JJ, Hellio R, Tavitian A, Louvard D (1994). A small rab GTPase is distributed in cytoplasmic vesicles in non polarized cells but colocalizes with the tight junction marker ZO-1 in polarized epithelial cells. J Cell Biol 124, 101–115.

Zahraoui A, Louvard D, Galli T (2000). Tight junction, a platform for trafficking and signaling protein complexes. J Cell Biol 151, F31–F36.

Zerial M, McBride H (2001). Rab proteins as membrane organizers. Nat Rev Mol Cell Biol 2, 107–117.